PAPER

Gain-assisted extraordinary optical transmission through periodic arrays of subwavelength apertures

New Journal of Physics
The open-access journal for physics

Gain-assisted extraordinary optical transmission through periodic arrays of subwavelength apertures

R Marani[1], A D'Orazio[2], V Petruzzelli[2], S G Rodrigo[3], L Martín-Moreno[4], F J García-Vidal[1,5] and J Bravo-Abad[1]

[1] Departamento de Física Teórica de la Materia Condensada, Universidad Autónoma de Madrid, E-28049 Madrid, Spain
[2] Dipartimento di Elettrotecnica ed Elettronica, Politecnico di Bari, via re David 200, 70125 Bari, Italy
[3] Institute of Optics, University of Rochester, Rochester, NY 14627, USA
[4] Instituto de Ciencia de Materiales de Aragón and Departamento de Física de la Materia Condensada, CSIC—Universidad de Zaragoza, E-50009 Zaragoza, Spain
E-mail: fj.garcia@uam.es

New Journal of Physics **14** (2012) 013020 (16pp)
Received 14 October 2011
Published 13 January 2012
Online at http://www.njp.org/
doi:10.1088/1367-2630/14/1/013020

Abstract. We theoretically investigate the amplification of extraordinary optical transmission (EOT) phenomena in periodic arrays of subwavelength apertures incorporating gain media. In particular, we consider a realistic structure consisting of an opaque silver film perforated by a periodic array of slits and clad on each side by an optically pumped dielectric thin film containing rhodamine dye molecules. By solving the semiclassical electronic rate equations coupled to rigorous finite-element simulations of the electromagnetic fields, we show how the resonant electric-field enhancement associated with EOT properties enables complete ohmic loss compensation at moderate pump intensity levels. Furthermore, our calculations show that, as a consequence of the strong spatial hole-burning effects displayed by the considered structures, three separate regimes of operation arise: the system can behave as an absorber, an optical amplifier or a laser, depending on the value of the pump intensity. A discussion on the feasibility of reaching the lasing regime in the considered class of structures is also presented.

[5] Author to whom any correspondence should be addressed.

Contents

1. Introduction 2
2. Theoretical framework 3
3. Numerical results and discussion 6
4. Conclusions 14
Acknowledgment 15
References 15

1. Introduction

The resonant transmission of light through subwavelength apertures in metal films has been the subject of considerable research activity over the last 10 years [1, 2]. The physics underlying extraordinary optical transmission (EOT) properties relies essentially on the ability of surface plasmons (SPs) to create significant electric field enhancements at the interfaces of the metallic film. This field enhancement assists externally incident light to be funneled through subwavelength apertures, yielding much larger transmission coefficients than those expected from the classical theory of diffraction [3, 4]. The key role played by SPs in this process makes, on the one hand, EOT phenomena natural candidates as the basis for a number of applications in which the subwavelength confinement of the electromagnetic (EM) field is a crucial ingredient. However, on the other hand, the large ohmic losses exhibited by SPs in the optical regime (even in the case of noble metals) represent a fundamental limitation that reduces drastically the practical applicability of EOT properties.

The above-mentioned drawback can actually be viewed as a more general challenge faced by any nanophotonic phenomena relying on the subwavelength confinement of an electric field close to a metallic surface. Recently, the incorporation of optically or electrically pumped gain media (dye molecules, quantum wells or dots, etc) was proposed as a possible route to solve the limitation introduced by ohmic losses in the performance of nanoplasmonic systems, including plasmonic waveguides and metamaterials [5–21]. In this approach, the external EM cavity present in most conventional active devices (which provides the optical feedback needed for amplification or lasing action in those systems [22]) is replaced by the strong EM field confinement properties associated with SPs. More specifically, the large local electric field enhancement associated with the plasmonic resonances supported by the system induces a substantial increase of the interaction strength between the external EM radiation and the gain medium. As a consequence, the effective gain coefficient of the system is dramatically boosted (compared to the gain coefficient displayed by the same active material in bulk) to the extent that full compensation of ohmic losses was reported recently in fishnet-like metamaterials [17]. In this context, despite its significant fundamental and applied interest, a detailed analysis of the generalization of the above-described ideas to loss compensation in EOT phenomena is lacking.

The aim of this paper is to theoretically study optical amplification of EOT properties in periodic arrays of subwavelength apertures incorporating optically pumped gain media. Specifically, we consider a realistic structure formed by a periodic array of subwavelength slits perforated in an optically thick silver metallic film and sandwiched between two thin layers of a dielectric containing rhodamine dye molecules. We assume that such a structure is illuminated by means of a canonical pump–probe configuration. The theoretical framework

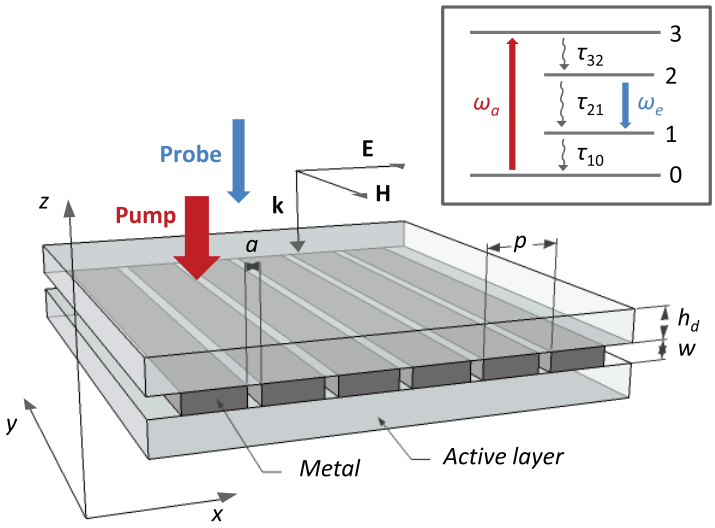

Figure 1. Sketch of the active structure analyzed in this work. The inset shows the energy level diagram, and the corresponding electronic transitions and lifetimes, of the four-level model used to describe the interaction between external radiation and the active regions of the system.

applied in this paper consists essentially in extending the traditional frequency-domain analysis of gain amplification and lasing action [22, 23] to structures displaying a highly non-uniform gain distribution at the subwavelength scale. In order to do that, we generalize recent works in this context [7, 11, 14] and solve the electronic rate equations of a four-level model of the active medium coupled to rigorous electrodynamical calculations of both the pump and probe obtained by means of the finite-element method (FEM). Using this theoretical framework, the response of the considered class of structures is probed by analyzing how its steady-state spectral response depends on the pump beam intensity. The corresponding results are then explained in terms of the evolution with the pump intensity of the spatial distribution of the electronic population inversion in the active regions of the structure. Our numerical results show that, for realistic configurations, full compensation of ohmic losses can be achieved by using moderate pump intensities below the damage threshold of the system. Our simulations also allow us to distinguish three different regimes of operation that arise as the pump intensity is increased: the whole structure can behave as an absorber, an optical amplifier or a laser. In this paper, we also provide a discussion on how lasing action could be achieved in realistic configurations.

This paper is organized as follows. In section 2, a description of the investigated structures is presented, together with an outline of the theoretical model used in our numerical experiments. Section 3 is devoted to the analysis of loss compensation and optical amplification in the considered class of structures. Final conclusions and remarks are presented in section 4.

2. Theoretical framework

We consider the active structure shown in figure 1. It consists of a periodic array (period p) of subwavelength slits of width a milled on a silver metallic film of thickness w. The slit array is

sandwiched between two dielectric thin films of width h_d containing rhodamine dye molecules, which, when optically pumped, act as a gain medium. Air regions extend infinitely above and below the whole structure. We also assume that the considered system is illuminated by means of a generic pump–probe configuration. In this configuration, part of the EM energy of a pump field (specifically, the energy carried by one of its Fourier components at a frequency $\omega = \omega_p$) is transferred to the Fourier component of a probe field at a different frequency $\omega = \omega_s$ (usually, $\omega_p > \omega_s$) via the variation of atomic potential energy occurring inside a suitably chosen gain medium.

To accurately model the interplay between the different physical mechanisms involved in this problem, we employ a theoretical framework based on a frequency-domain approach. This kind of theoretical analysis has been extensively applied to describe optically pumped gain media both in the context of traditional active dielectric structures [22, 23], as well as, more recently, in the context of gain and lasing action in plasmonic waveguides and metamaterials [7, 11, 14, 17]. In what follows we summarize the particular numerical implementation of this framework employed in this paper.

Firstly, to describe the electronic dynamics of the rhodamine dye molecules, we assume that their corresponding electronic energy levels and transition rates can be accounted for by a four-level system (see schematics in the inset of figure 1). This approximation has shown its accuracy to model optical gain induced by the considered class of active dyes [24]. Under this assumption, the whole EM response of the structure under continuous-wave (cw) excitations can be obtained by solving the following set of linearly coupled partial differential equations, which govern the spatio-temporal dynamics of the electronic population densities ($N_i(\mathbf{r}, t)$, $i = 0, 1, 2, 3$) of each of the energy levels displayed in the inset of figure 1 [22]:

$$\frac{\partial N_3(\mathbf{r}, t)}{\partial t} = W_a(\mathbf{r})\,[N_0(\mathbf{r}, t) - N_3(\mathbf{r}, t)] - \frac{N_3(\mathbf{r}, t)}{\tau_{32}}, \tag{1}$$

$$\frac{\partial N_2(\mathbf{r}, t)}{\partial t} = -W_e(\mathbf{r})\,[N_2(\mathbf{r}, t) - N_1(\mathbf{r}, t)] + \frac{N_3(\mathbf{r}, t)}{\tau_{32}} - \frac{N_2(\mathbf{r}, t)}{\tau_{21}}, \tag{2}$$

$$\frac{\partial N_1(\mathbf{r}, t)}{\partial t} = W_e(\mathbf{r})\,[N_2(\mathbf{r}, t) - N_1(\mathbf{r}, t)] + \frac{N_2(\mathbf{r}, t)}{\tau_{21}} - \frac{N_1(\mathbf{r}, t)}{\tau_{10}}, \tag{3}$$

$$\frac{\partial N_0(\mathbf{r}, t)}{\partial t} = -W_a(\mathbf{r})\,[N_0(\mathbf{r}, t) - N_3(\mathbf{r}, t)] + \frac{N_1(\mathbf{r}, t)}{\tau_{10}}, \tag{4}$$

where τ_{ij} ($i, j = 0, 1, 2, 3$) are the lifetimes of the non-radiative transitions between the ith and the jth energy levels. $W_a(\mathbf{r})$ and $W_e(\mathbf{r})$ control the radiative stimulated absorption and emission transitions in the system (i.e. they determine the exchange of energy between the gain medium and its EM surroundings) at frequencies ω_a and ω_e, respectively (see the definition of these frequencies in the inset of figure 1). For the pump–probe configuration considered in this work, these functions can be expressed as

$$W_{a,e}(\mathbf{r}) = \frac{\sigma_{a,e}(\omega_{p,s})\,\epsilon_0\,c\,n_{p,s}}{2\,\hbar\,\omega_{a,e}}\left|\mathbf{E}(\mathbf{r};\,\omega_{p,s})\right|^2 \tag{5}$$

with $n_{p,s}$ being the value of the refractive index of the gain composite (i.e. the dielectric host and the dye molecules embedded in it) at the pump (probe) frequency $n_{p,s} = n(\omega_{p,s})$. $\mathbf{E}(\mathbf{r};\,\omega_{p,s})$ stand for the spatial profile of the Fourier component of the electric field in the structure at the pump and probe frequencies. ϵ_0 and c are the free space permittivity and the speed of light in

vacuum, respectively. Finally, the functions $\sigma_{a,e}(\omega)$ represent the absorption and emission cross sections of the dye. These magnitudes can be written in terms of the corresponding normalized lineshapes as $\sigma_{a,e}(\omega) = \sigma_{a,e}^{(0)} L_{a,e}(\omega)$. The constants $\sigma_{a,e}^{(0)}$ control the overall quantum yield q of the gain process $q = \sigma_e^{(0)}/\sigma_a^{(0)}$. Note that, owing to the fact that these lineshape functions $L_{a,e}(\omega)$ peak at $\omega = \omega_{a,e}$, the efficiency of the transfer of energy between the pump and probe pulses is maximal when the pump and probe central frequencies are tuned to the absorption and emission frequencies, respectively.

As described above, a crucial ingredient of the present formalism is the calculation of the EM field profile for both pump and probe wavelengths, $\mathbf{E}(\mathbf{r}; \omega_{p,s})$. Here those fields are obtained by means of the FEM (Comsol Multiphysics package), which models Maxwell's equations exactly, except for the discretization. In these simulations, the dielectric constant used to describe the metallic regions of the system, $\epsilon_m(\omega)$, is given by a canonical Drude response with a Lorentzian resonance,

$$\epsilon_m(\omega) = \epsilon_\infty - \frac{\omega_p^2}{\omega^2 + i\,\gamma\omega} - \frac{\Delta\epsilon_L \omega_L^2}{\omega^2 - \omega_L^2 + i\,\gamma_L\omega}, \tag{6}$$

where ϵ_∞ is the non-resonant permittivity. ω_p and γ are the plasma frequency and the relaxation rate of the metal under consideration, respectively. The parameters of the Lorentz oscillator are the oscillator strength $\Delta\epsilon_L$, the resonant frequency ω_L and the damping constant γ_L.

We now turn to the analysis of the steady-state solutions of equations (1)–(4). In general, a time-domain approach would be necessary to track the whole spatio-temporal dynamics described by that set of equations [13, 18, 25–29]. However, if the duration of the external field pulses is much longer than the time scale needed to access the steady-state values of the electronic population densities, a cw theoretical approach can be employed to describe the optical response of the analyzed system with accurate precision. In addition, in the operation regimes considered in this paper, the physics underlying optical amplification can be fully accounted for in terms of just the steady-state behavior of the system. This also allows us to increase significantly the computational efficiency of our calculations with respect to those performed in a time-domain analysis. Specifically, by taking the limit $\partial N_i(\mathbf{r}, t)/\partial t \to 0$ in the set of equations (1)–(4), after some straightforward algebra, one can find that the steady-state population inversion $\Delta N(\mathbf{r})$ of the stimulated emission electronic transition (the one between energy levels 2 and 1) can be expressed as

$$\Delta N(\mathbf{r}) = N_{TOT} \frac{\Omega_a(\mathbf{r})\,[\Omega_e(\mathbf{r}) - 1]}{[\Omega_a(\mathbf{r}) + \Omega_e(\mathbf{r})]\,[\Omega_a(\mathbf{r}) + 1]}, \tag{7}$$

where N_{TOT} is the total density of dye molecules present in the system. The functions $\Omega_a(\mathbf{r})$ and $\Omega_e(\mathbf{r})$ are defined as $\Omega_a(\mathbf{r}) = 1/[1 + (W_a(\mathbf{r})\tau_{10})^{-1}]$ and $\Omega_e(\mathbf{r}) = (\tau_{21}/\tau_{10})[1 + W_e(\mathbf{r})\tau_{10}]/[1 + W_e(\mathbf{r})\tau_{21}]$. As can be deduced from equation (7), the dependence of $\Delta N(\mathbf{r})$ on both the pump and probe E-field profiles enters through the dependence of $W_a(\mathbf{r})$ and $W_e(\mathbf{r})$ on the corresponding field intensities, $|\mathbf{E}(\mathbf{r}; \omega_p)|^2$ and $|\mathbf{E}(\mathbf{r}; \omega_s)|^2$, respectively (see equation (5)).

Now, in most active materials that can be described by a four-level system (including the active dye considered in this paper), the stimulated emission transition is orders of magnitude slower than the other electronic transitions occurring in the system, i.e. $\{\tau_{32}, \tau_{10}\} \ll \tau_{21}$. This fact allows us to rewrite equation (7) in a more compact way, namely

$$\Delta N(\mathbf{r}) = N_{TOT} \frac{W_a(\mathbf{r})\tau_{21}}{1 + [W_a(\mathbf{r}) + W_e(\mathbf{r})]\tau_{21}}. \tag{8}$$

Once $\Delta N(\mathbf{r})$ is computed, the complex permittivity of the active material $\epsilon_g(\mathbf{r})$ at a frequency ω_s can be obtained from the following expression [11, 14, 22]:

$$\epsilon_g(\mathbf{r}, \omega_s) = \epsilon'_g(\omega_s) + i\frac{c}{\omega_s}[\epsilon'_g(\omega_s)]^{1/2}\,[\alpha(\mathbf{r}, \omega_s) - g(\mathbf{r}, \omega_s)], \tag{9}$$

where $\epsilon'_g(\omega)$ is the relative permittivity of the considered gain composite (i.e. the dielectric material hosting the molecules and the molecules themselves). $\alpha(\mathbf{r}, \omega_s) = \sigma_a(\omega_s)N_0(\mathbf{r})$ and $g(\mathbf{r}, \omega_s) = \sigma_e(\omega_s)N_2(\mathbf{r})$ are the local absorption and gain coefficients, respectively.

As can be deduced from equation (9), in general, a self-consistent approach would be needed to compute the interaction of the gain medium and the pump–probe illumination. The optical pumping increases the gain coefficient of the whole structure, which varies the complex permittivity of the system. In turn, this change in $\epsilon_g(\mathbf{r}, \omega_s)$ modifies the interaction between the pump and the gain material, which can modify the original assumption on how the pump and the probe were interacting with the dye molecules. However, although this is the most general scenario, for all the cases considered in this paper, this self-consistent approach can be simplified to a simpler two-step problem [11, 14]. Specifically, as we show in this work, for the class of structures considered here, and for pump and probe intensities below the damage threshold of the system, one finds that $\sigma_a^{(0)}\mathbf{E}(\mathbf{r}; \omega_p) \gg \sigma_e^{(0)}\mathbf{E}(\mathbf{r}; \omega_s)$. By applying this condition to equation (8), it is straightforward to conclude that the effect of the probe beam on the population inversion $\Delta N(\mathbf{r})$ is negligible, and that, consequently, the two-step approach considered here gives virtually the same results as those obtained by using a full self-consistent calculation.

3. Numerical results and discussion

The active medium considered in our simulations consists of a dielectric host material (of refractive index $n_h = 1.62$) doped with rhodamine 800 (Rh800) dye molecules. The total density of dye molecules embedded in the host dielectric is assumed to be $N_{TOT} = 6 \times 10^{18}\,\mathrm{cm}^{-3}$ [17, 18]. The parameters defining the response of the dye molecules are taken from available experimental data [17, 18]. Specifically, the absorption and emission cross sections of each molecule have a Lorentzian shape defined by the same half-widths, $\Gamma_a = \Gamma_e = 1/(20\,\mathrm{fs})$, and are centered at $\lambda_a = 680\,\mathrm{nm}$ and $\lambda_e = 710\,\mathrm{nm}$, respectively. The values of the maxima absorption and emission cross sections are $\sigma_a^{(0)} = 3.14 \times 10^{-16}\,\mathrm{cm}^2$ and $\sigma_e^{(0)} = 2.43 \times 10^{-16}\,\mathrm{cm}^2$ (see the definition of these magnitudes in section 2). The stimulated emission lifetime is $\tau_{21} = 500\,\mathrm{ps}$. This value for τ_{21} corresponds to a bulk configuration. The calculation of the possible position-dependent variation of τ_{21} due to the presence of the metallic regions forming the considered structure represents a computational tour-de-force that is outside the scope of the present simulations. On the other hand, the metallic regions of the considered system are assumed to be made of silver. Thus, the following values are used in the expression for dispersion relation given in equation (6): $\epsilon_\infty = 4.6$, $\omega_p = 9.0\,\mathrm{eV}$, $\gamma = 0.07\,\mathrm{eV}$, $\omega_L = 4.9\,\mathrm{eV}$, $\gamma_L = 1.2\,\mathrm{eV}$ and $\Delta\epsilon_L = 1.10$ [18, 30]. In the rest of this paper, we refer to the structure in which the total density of dye molecules embedded in the host dielectric layers is negligible as the *passive* structure.

The computational domain used in our FEM simulations is bounded by perfectly matched layers along the z-direction (see the definition of axes in figure 1), whereas periodic boundary conditions are applied along the x-direction. The defined computational window is then sampled by a non-uniform mesh whose maximum element size is more than 15 times smaller than

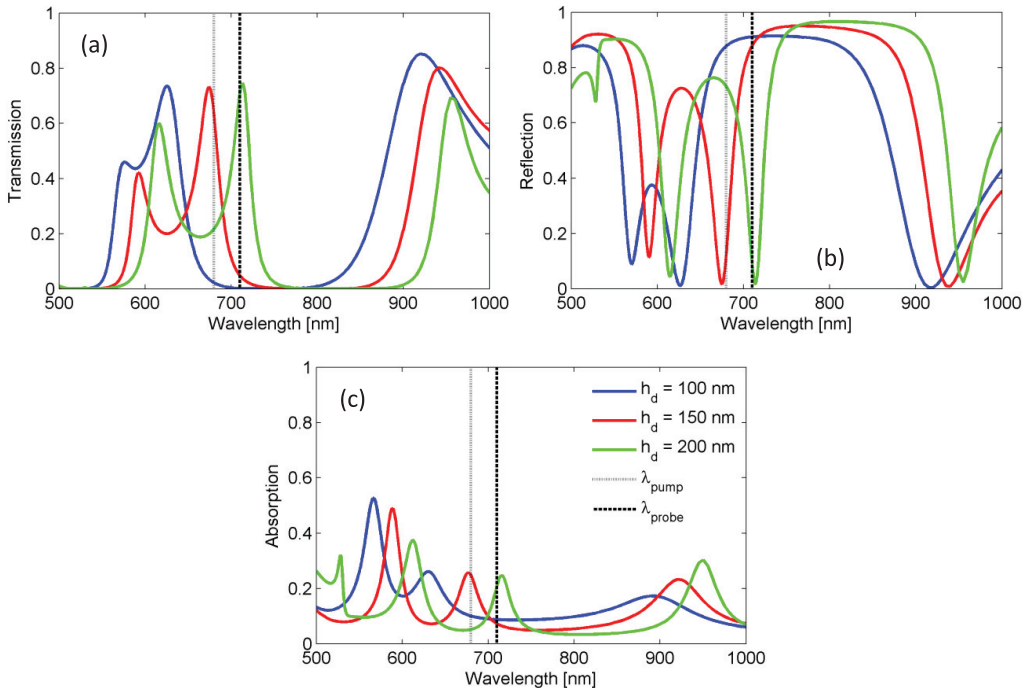

Figure 2. (a) Spectral response of the studied passive infinite array of slits milled on a silver film, as a function of the thickness h_d of the dielectric layers cladding the array. Transmission, reflection and absorption spectra are shown in panels (a), (b) and (c), respectively. Dotted and dashed vertical lines in each panel mark the wavelengths of pump and probe signals, respectively.

the operation wavelength. In addition, we note that the transmission and reflection spectra shown in this paper were obtained by integrating the flow of the Poynting vector through line monitors properly placed below and above the air–dielectric interfaces and parallel to them. The corresponding absorption spectrum is then obtained just by subtracting, at each wavelength, transmission and reflection from unity.

Figure 2 renders the results from a first set of simulations in which the spectral response of the passive case is computed for several values of the thickness h_d of the dielectric layers cladding the metallic array. The geometrical parameters defining the metallic slit array considered in these simulations are $w = 150$ nm, $p = 520$ nm and $a = 100$ nm (see the definition of these parameters in figure 1). As we show below, these geometrical parameters are optimized so that the main SP resonance supported by slit array is tuned to the stimulated emission wavelength ($\lambda_e = 710$ nm). In addition, to maximize the whole optical amplification process, all simulations are performed assuming that the pump and probe signals are centered at λ_a and λ_e, respectively. This optimization of the geometrical parameters of the structure can be viewed as a particular implementation of the above-mentioned general approach to loss compensation in nanophotonics, consisting in controlling the optical response of a structure by tuning its plasmonic resonance to an electronic radiative transition of a suitably chosen class of molecules embedded in the system.

As shown in figure 2, the spectra computed for each value of h_d are dominated by the presence of three main resonances. The physical origin of these resonant features emerges

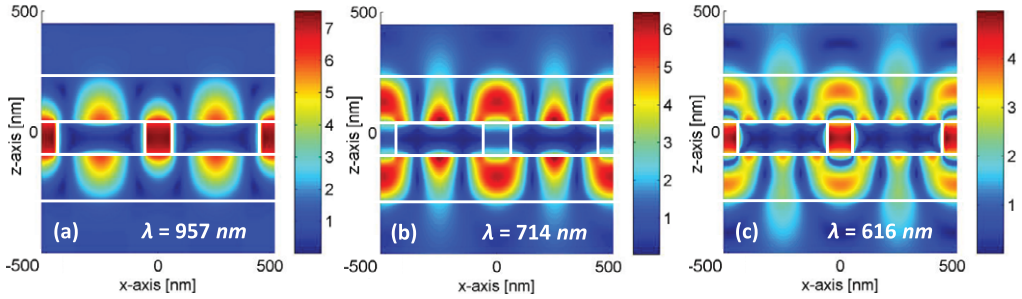

Figure 3. Spatial profile of the modulus of the y component of the magnetic field, $|H_y|$, normalized to the saturation magnetic field, $|H_{\rm th}| = |E_{\rm th}|/\eta_0$, with η_0 being the free space impedance. Panels (a), (b) and (c) correspond to wavelengths $\lambda = 957$ nm, $\lambda = 714$ nm and $\lambda = 616$ nm, respectively.

when looking at the corresponding EM field profiles. Specifically, figure 3 renders the three on-resonance H_y field profiles, as computed for the case $h_{\rm d} = 200$ nm (green lines in figure 2). These results suggest that two of the resonances (the ones appearing at $\lambda = 957$ nm and $\lambda = 616$ nm, displayed in figures 3(a) and (c), respectively) are linked to localized EM resonances (Fabry–Perot resonances) supported by the slits [31]. In contrast, as revealed by figure 3(b), the resonance located at $\lambda \approx 710$ nm confines most of the field near the metal–dielectric interfaces, and thereby its physical origin can be linked to the presence of SPs decorating the interfaces of the slit array [31]. This fact makes this latter resonance the optimal candidate for enhancing the interaction between the external radiation and the dye molecules embedded in the considered class of structures. Moreover, as observed in figure 2, the spectral location of this resonance is rather sensitive to small variations of $h_{\rm d}$, which allows us to easily tune the resonance to the stimulated electronic transition of the gain medium. For the specific structure and gain medium considered in this paper, the optimal thickness of the dielectric layers is $h_{\rm d} = 200$ nm (see figure 2). Thus, in the rest of the paper we assume this value for $h_{\rm d}$. We point out that, although it is outside the framework of the fundamental analysis presented here, further enhancement of the interaction between external radiation and the active medium could be achieved by optimizing the structure so that $\lambda_{\rm a}$ and $\lambda_{\rm e}$ are simultaneously tuned to two SP resonances of the system.

Figure 4 summarizes our numerical results on how the spectral response of the considered structure is modified when optically pumped dye molecules are embedded in the top and bottom dielectric layers sketched in figure 1. In these simulations, we assume the same geometrical parameters as those given above for the passive system. Note also that all the electric-field magnitudes are normalized to the magnitude of the saturation electric field, defined as $|E_{\rm th}| = 2\hbar\omega_{\rm a}/(\epsilon_0 c n' \tau_{21} \sigma_{\rm a}^{(0)})$ (where $\hbar$ is the reduced Planck constant and n' is the refractive index of gain composite, $n' = (\epsilon_{\rm g}')^{1/2}$). For a given set of parameters describing the electronic four-level system, the value of $|E_{\rm th}|$ corresponds to the magnitude of the pump electric field ($|E_{\rm in}|$) at which the electronic population of the ground is depleted to one half of its initial value (i.e. at which $N_0 = 0.5 \times N_{\rm TOT}$).

Figures 4(a)–(c) clearly demonstrate that the system displays two notably different responses as a function of the optical pumping strength. For values of $|E_{\rm in}|$ such that $|E_{\rm in}| < |E_{\rm th}|$, the whole structure behaves essentially as an optical absorber centered at the stimulated emission wavelength. This is clearly visualized in the absorption peak centered at $\lambda_{\rm e}$ observed

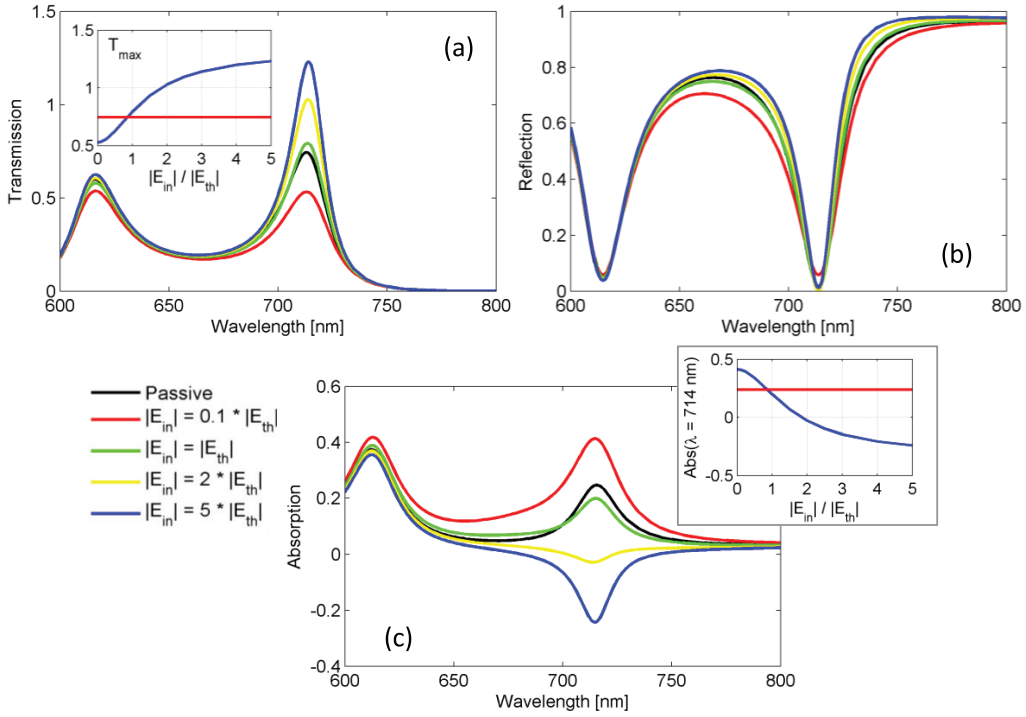

Figure 4. (a) Transmission, (b) reflection and (c) absorption spectra characterizing the considered active structure, as computed for several values of the input electric field intensity $|E_{\mathrm{in}}|$. For comparison the results corresponding to the passive case are also plotted (black lines). The inset of figure 4(a) shows the variation of the maximum of transmission at resonance as a function of the ratio $|E_{\mathrm{in}}|/|E_{\mathrm{th}}|$. The red line in this inset marks the value of the maximum transmission corresponding to the passive case. The inset of figure 4(c): the same as the inset of figure 4(a), but now the results correspond to absorption at the resonant wavelength, $\lambda = 714$ nm.

in figure 4(c) for the case $|E_{\mathrm{in}}|/|E_{\mathrm{th}}| = 0.1$. Note that the resonant peak located at $\lambda \approx 620$ nm is barely influenced by the optical pumping, essentially because the corresponding wavelength is shifted away from the center of the gain profile. As the value of $|E_{\mathrm{in}}|$ is increased, the absorption peak starts smearing out (see figure 4(c)), until the characteristics of the transmission and reflection spectra of the passive system are fully recovered by the active one. We have found numerically that, in the considered structure, this occurs when $|E_{\mathrm{in}}|/|E_{\mathrm{th}}| \approx 0.9$ (see the insets of figures 4(a) and (c)).

Now, as shown in figure 4(a), if the value of $|E_{\mathrm{in}}|$ is further increased, the EM power generated through the pump–probe frequency conversion taking place inside the gain medium starts compensating for the intrinsic ohmic losses present in the system (i.e. the absorption losses due to the penetration of the EM field into the metallic regions). The loss-compensation process flattens the absorption peak centered at λ_{e} (see the main and inset panels in figure 4(c)), and leads to values of the maximum transmission at resonances larger than those found in the passive structure (see the inset of figure 4(a)). This dependence of the spectral response on $|E_{\mathrm{in}}|$

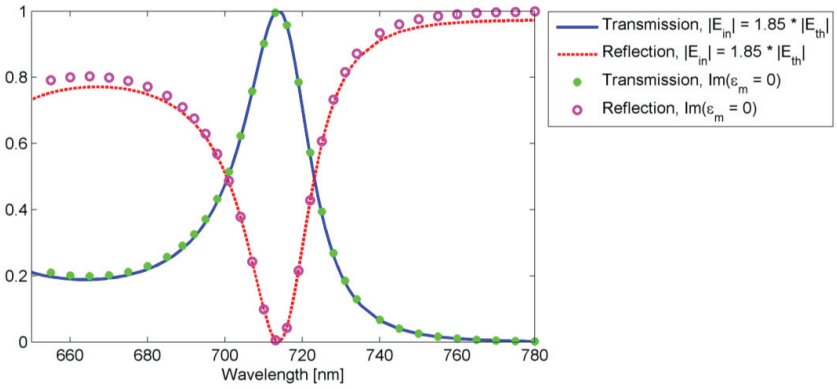

Figure 5. Transmission (blue solid line) and reflection (red dashed line) spectra computed for the case $|E_{\mathrm{in}}|/|E_{\mathrm{th}}| = 1.85$. Green dots and magenta circles show the results of a series of simulations in which the metallic regions of the structure are assumed to behave as perfect metals (i.e. in which $\mathrm{Im}(\epsilon_{\mathrm{m}}) = 0$).

continuously evolves as the pump field is further increased, up to a value of $|E_{\mathrm{in}}|$ at which the optical pumping is large enough to completely compensate for the ohmic losses present in the structure. In the analyzed system, this condition is reached when $|E_{\mathrm{in}}|/|E_{\mathrm{th}}| \approx 1.9$.

Importantly, when complete ohmic loss compensation occurs, 100% transmission is achieved at $\lambda = \lambda_{\mathrm{e}}$. This result is linked to the full transmission properties observed in EOT phenomena occurring in metals that behave as perfect metals (i.e. in which $\mathrm{Im}(\epsilon_{\mathrm{m}}) = 0$) [4, 32]. To investigate this point in more detail, we have compared the numerical results obtained for the active structure operating at $|E_{\mathrm{in}}|/|E_{\mathrm{th}}| \approx 1.9$ with those corresponding to a passive structure in which the condition $\mathrm{Im}(\epsilon_{\mathrm{m}}) = 0$ is artificially imposed. Figure 5 shows the comparison between the transmission and reflection spectra obtained for each case. The excellent agreement found between both calculations demonstrates that, owing to the action of the gain medium, the system does effectively act as a passive system in which the silver regions are replaced by perfect metal areas.

For values of the pump field magnitude larger than those corresponding to complete ohmic loss compensation, the action of the gain medium induces the considered system to effectively behave as an optical amplifier [23]. This is clearly illustrated in figure 4(c), which shows that for $|E_{\mathrm{in}}| > 1.9|E_{\mathrm{th}}|$, negative values of absorption are obtained in a wavelength interval centered at $\lambda = \lambda_{\mathrm{e}}$. Note that, due to the physical limit set by the damage threshold of the structure, values of $|E_{\mathrm{in}}|$ larger than $5|E_{\mathrm{th}}|$ would lead to unrealistic predictions [14]. As displayed in figure 4(a), in this optical amplification regime, the values of maximum transmission at resonance can be significantly larger than unity. As discussed below, this fact opens up the possibility of inducing lasing action in the system. We also note that, by comparing figures 4(a) and (b), it can be deduced that, within this optical amplification regime, most of the optical power generated in the gain medium ends up being redirected to the transmission region rather than to the reflection region. This could also be an important factor that facilitates the practical implementation of the results discussed in this paper.

Further physical insight into this problem can be obtained by analyzing how the evolution with the pump intensity of the effective response of the system can be accounted for in terms of

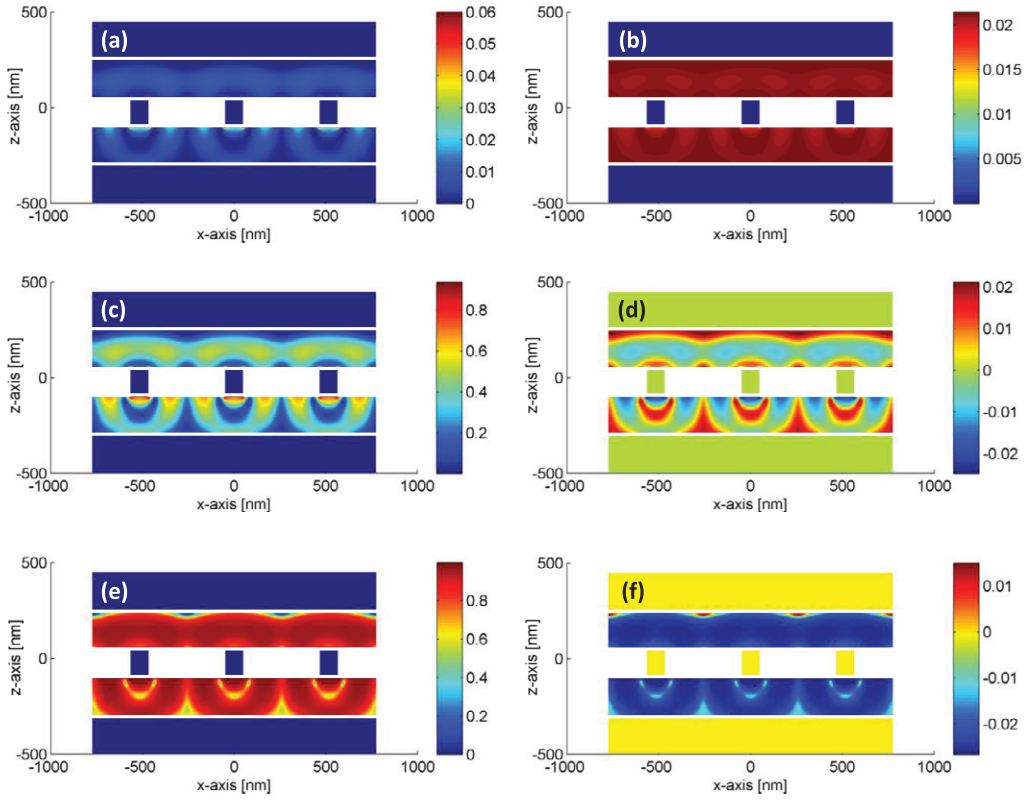

Figure 6. Left column: spatial profile of the normalized population inversion density $\Delta N/N_{\mathrm{TOT}}$ computed for (a) $|E_{\mathrm{in}}|/|E_{\mathrm{th}}| = 0.1$, (c) $|E_{\mathrm{in}}|/|E_{\mathrm{th}}| = 1$ and (e) $|E_{\mathrm{in}}|/|E_{\mathrm{th}}| = 5$. Right column: spatial profile of the calculated imaginary part of the dielectric function corresponding to the same series of $|E_{\mathrm{in}}|/|E_{\mathrm{th}}|$ considered in the left column. In all calculations $\lambda = 710\,\mathrm{nm}$ is assumed.

the corresponding variation of the population inversion spatial profile $\Delta N(\mathbf{r})$. Figure 6 renders the results for spatial distribution of the population inversion, normalized to N_{TOT} (panels (a), (c) and (e)), and the corresponding imaginary part of the dielectric constant inside the dielectric layers (right column, panels (b), (d) and (f)). Three different values of the pump electric-field magnitude are considered in this figure. Figures 6(a) and (b) correspond to $|E_{\mathrm{in}}|/|E_{\mathrm{th}}| = 0.1$, figures 6(c) and (d) display the results for $|E_{\mathrm{in}}|/|E_{\mathrm{th}}| = 1$, while in figures 6(e) and (f) $|E_{\mathrm{in}}|/|E_{\mathrm{th}}| = 5$ is assumed. These values for $|E_{\mathrm{in}}|/|E_{\mathrm{th}}|$ correspond to three representative spectral responses of the system (see the red, green and blue lines in the spectra shown in figure 4). All the results displayed in figure 6 have been computed at the stimulated emission wavelength, $\lambda_{\mathrm{e}} = 710\,\mathrm{nm}$.

Figure 6(a) shows how, for the lowest magnitude of the incident electric field, the density of inverted dye molecules is negligible in nearly every position inside the active regions of the structure. As a consequence, these active regions act effectively as an almost uniform absorbing material with its resonance centered at $\lambda = \lambda_{\mathrm{e}}$ (see figure 6(b)). In contrast, for $|E_{\mathrm{in}}|/|E_{\mathrm{th}}| = 1$, the response of the system changes substantially, and the active dielectric regions display some *hot-spots* in which a significant density of inverted molecules is found (see figure 6(c)). These regions are mainly located near the metallic interfaces of the slit array, basically because

it is precisely in those regions where significant values of electric-field enhancement are reached. The corresponding spatial distribution of ϵ_g shows that in these regions of maximal population inversion, the sign of the absorption coefficient changes from positive to negative (see figure 6(d)), i.e. the active medium acts locally as the gain medium in those regions. The effective response of active dielectric layers is then determined by the spatial average (weighted by the electric-field intensity) of the contribution to the absorption coefficient of the absorbing and gain regions. In particular, for $|E_{in}|/|E_{th}| = 1$ this average is approximately zero, which explains why in this case the spectral response of the structures coincides with that of the passive system (see figure 4). For the largest value of $|E_{in}|$ considered here ($|E_{in}|/|E_{th}| = 5$), the optical pumping is so strong that the regions displaying significant population inversion occupy almost completely the whole volume defined by the top and bottom dielectric layers. Thus, as seen in figure 6(e), in this operation regime, these layers can be effectively considered as formed by a uniform optical amplifying medium. Importantly, note the crucial role played by the high non-uniformity of EM field distributions in determining the effective response of the system. Specifically, as discussed above, this non-uniformity induces the presence of *spatial holes* in the gain medium. In these spatial holes, the local population inversion is not saturated, or alternatively, the population inversion density is smaller than in the regions of maximum electric field intensity. This occurs much in the same way as in the well-known *spatial hole-burning* processes observed in traditional active and lasing systems [22, 23]. Thus, we believe that the results reported in this paper can be considered as a novel instance of how spatial hole-burning effects at the subwavelength scale can be responsible for the effective response of an active nanophotonic structure.

Finally, to quantitatively characterize the different operation regimes described above, we analyze how the total decay rate of the EM energy stored in the considered active structure can be decomposed into the different absorption and gain *channels* governing the effective response of the system. As we discuss below, this analysis also allows us to investigate the conditions under which the studied systems can display lasing action at the subwavelength scale. Specifically, the total decay rate of the structure (Γ_T) can be expressed as a function of the pump E-field magnitude $|E_{in}|$ as

$$\Gamma_T(|E_{in}|) = \Gamma_{rad} + \Gamma_{Ohm} + \Gamma_{Rh800} - \Gamma_g(|E_{in}|), \tag{10}$$

where Γ_{rad} and Γ_{Ohm} are the decay rates corresponding to the intrinsic radiation and ohmic losses present in the system, respectively. Γ_{Rh800} is the decay rate associated with the absorption of the dye molecules in the absence of external pumping. Note that Γ_{ohm}, Γ_{rad} and Γ_{Rh800} are only determined, respectively, by material properties of the slit array (ohmic losses), by the geometry of the system (radiation losses) and by intrinsic properties of the rhodamine molecules (the linewidth and maximum value of the corresponding absorption cross section). Therefore, these three magnitudes are independent of $|E_{in}|$. On the other hand, the function $\Gamma_g(|E_{in}|)$ determines the rate at which the external EM energy is pumped into the system (thereby it has the opposite sign from Γ_{rad}, Γ_{ohm} and Γ_{Rh800} in equation (10)); this magnitude obviously satisfies $\Gamma_g(|E_{in}| = 0) = 0$.

The value of Γ_{rad} can be easily obtained from the linewidth of the resonant transmission peak observed at $\lambda = \lambda_e$ in the case of the passive structure in which the condition $\mathrm{Im}(\epsilon_m) = 0$ is imposed (see figure 5). Once the value of Γ_{rad} is known, the calculation of Γ_{Ohm} is also

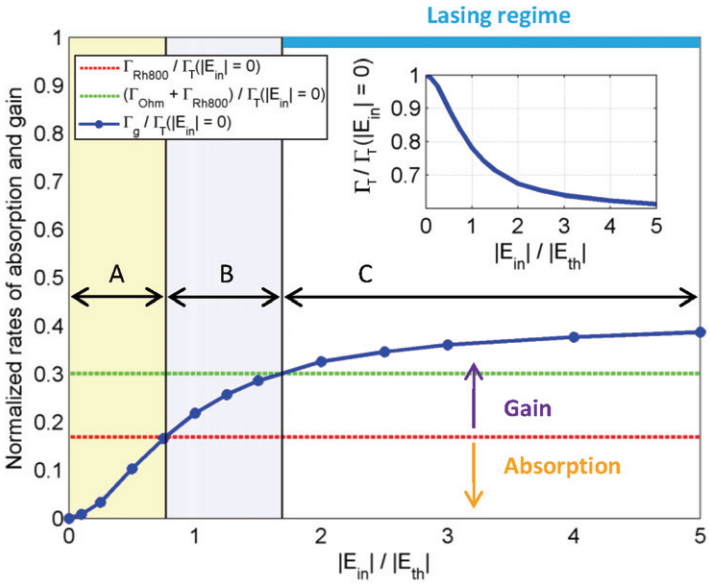

Figure 7. Normalized rate of gain $\Gamma_g/\Gamma_T(|E_{in}|=0)$ (blue line) as a function of the normalized pump electric field intensity ($|E_{in}|/|E_{th}|$). The dotted red line marks the values of the normalized molecular absorption rate, $\Gamma_{Rh800}/\Gamma(|E_{in}|=0)$, while the dotted green line corresponds to all intrinsic absorption losses present in the system, $(\Gamma_{Ohm}+\Gamma_{Rh800})/\Gamma(|E_{in}=0|)$. All rates are computed at $\lambda=710$ nm. Vertical down and up arrows define the regions in which the analyzed structure effectively behaves as an absorber and an optical amplifier, respectively. The thick light blue line marks the onset of lasing action in the considered structure. The inset displays the normalized total decay rate, $\Gamma_T/\Gamma_T(|E_{in}|=0)$, versus the ratio $|E_{in}|/|E_{th}|$.

straightforward from the linewidth of the resonant transmission peak computed for the passive structure, now assuming a realistic ϵ_m in the metallic regions of the system (see the black line in figure 4). Finally, for fixed values of Γ_{rad} and Γ_{Ohm}, the value of Γ_{Rh800} can be readily deduced from the linewidth of the active system assuming no optical pumping (i.e. assuming $|E_{in}|=0$). Thus, once the values of Γ_{rad}, Γ_{Ohm} and Γ_{Rh800} have been computed, the dependence of Γ_g on $|E_{in}|$ can be obtained just by tracking how the linewidth of transmission resonance observed in the active structure evolves as $|E_{in}|$ is increased. Figure 7 renders the corresponding results for the described absorption and gain rates. In this figure, the decay rates are normalized to the total decay rate of the active system with no external pumping $\Gamma_T(|E_{in}|=0)$, which is given by $\Gamma_T(|E_{in}|=0)=\Gamma_{rad}+\Gamma_{Ohm}+\Gamma_{Rh800}$ (see equation (10)). The horizontal red line in figure 7 marks the value of the normalized molecular absorption losses, $\Gamma_{Rh800}/\Gamma(|E_{in}|=0)$, while the green line corresponds to the normalized sum of all intrinsic absorption losses of the system $(\Gamma_{Ohm}+\Gamma_{Rh800})/\Gamma(|E_{in}=0|)$. Blue dots represent the calculated values of $\Gamma_g/\Gamma(|E_{in}=0|)$ for the corresponding values of $|E_{in}|/|E_{th}|$ displayed in the figure.

As illustrated in figure 7, three different intervals of operation (labeled as A, B and C) emerge from this analysis. For the values of $|E_{in}|/|E_{th}|<0.8$ (yellow region in figure 7), we obtain $\Gamma_g<\Gamma_{Rh800}$. This interval corresponds to the above-described low-pumping regime,

in which the gain medium effectively behaves as an absorbing material. For values of $|E_{in}|$ such that $0.8 < |E_{in}|/|E_{th}| < 1.6$ (cyan region in figure 7), Γ_g becomes larger than Γ_{Rh800} and, consequently, it contributes to reduce the total linewidth of the considered transmission resonance (see equation (10) and the inset of figure 7). From a physical point of view, these results suggest that, for low pump intensities, the EM energy from the active medium is first *invested* in compensating for the absorption losses associated with the dye molecules (interval A in figure 7). Once those losses have been compensated for, the pump–probe frequency conversion process taking place inside the gain medium starts compensating for the ohmic losses stemming from the penetration of the EM in the metallic regions of the system (this regime is labeled B in figure 7). Following this reasoning, one expects that once all intrinsic absorption losses have been compensated for, further increase of $|E_{in}|$ would lead to a new regime in which the energy provided by the gain medium starts compensating for the leakage of energy due to the radiation losses. This is precisely what is observed in the interval C of figure 7. We note that the values of $|E_{in}|/|E_{th}|$ at which the crossover between the different regimes of operation takes place agree well with the predictions for the same values obtained previously from the analysis of the evolution with $|E_{in}|/|E_{th}|$ of the maximum transmission at resonance (see figure 4). From figure 7, it is also clear that the value of $\Gamma_g/\Gamma(|E_{in}| = 0)$ saturates far from unity. This is essentially due to the fact that the saturation of the gain occurs before all the losses present in the system are fully compensated. Importantly, this full compensation of losses actually determines the onset of lasing action in the considered structure (see the thick light blue line in figure 7), similarly to what occurs in the different plasmonic structures displaying lasing action reported in the recent literature [33–36]. In this context, in order to access the lasing regime, one can envision a system in which the radiation losses are dramatically decreased by, for instance, reducing the width of the apertures. Alternatively, the lasing region could be accessible to a configuration with a similar geometry as that shown in this paper, but in which the damage threshold is significantly increased and, in which, in addition, the dye molecules have been replaced by a different gain medium showing notably larger saturation electric field intensities.

4. Conclusions

In conclusion, we have theoretically studied loss compensation in EOT phenomena enabled by optically pumped active media. Specifically, we have analyzed the spectral response of an active structure formed by a periodic array of subwavelength slits milled in an optically thick silver metallic film and sandwiched between two thin dielectric layers including rhodamine dye molecules. The corresponding results have been accounted for in terms of the evolution with the pump field magnitude of the spatial distribution of the density of electronically inverted molecules present in the system. Our calculations have shown that, for a conventional pump–probe illumination, moderate values of the magnitude of the pump electric field can lead to full compensation of the absorption ohmic losses induced by the penetration of the field in the metallic regions. We have also reported on the existence of three main operation regimes for the analyzed system. For low values of pump field, the whole structure effectively behaves as an optical absorber centered at the stimulated emission wavelength. As the pump field is increased, the system starts behaving as a special class of optical amplifiers in which the EM energy provided by the gain medium is first invested in compensating for the ohmic losses. Once the ohmic losses are fully compensated, the energy provided by the

gain-assisted pump–probe frequency conversion process allows compensating also the radiation losses present in the structure. We have also quantitatively characterized the conditions that would lead to full compensation of both ohmic and radiation losses and therefore to the onset of lasing action in the considered class of structures.

Acknowledgment

This work was sponsored by the Spanish Ministry of Science and Innovation under the projects MAT2009-06609-C02 and CSD2007-046-NanoLight and by the Ramón-y-Cajal program (grant no. RyC-2009-05489).

References

[1] Genet C and Ebbesen T W 2007 *Nature* **445** 39
[2] Garcia-Vidal F J, Martin-Moreno L, Ebbesen T W and Kuipers L 2010 *Rev. Mod. Phys.* **82** 729
[3] Ebbesen T W, Lezec H J, Ghaemi H F, Thio T and Wolff P A 1998 *Nature* **391** 667
[4] Martin-Moreno L, Garcia-Vidal F J, Lezec H J, Pellerin K M, Thio T, Pendry J B and Ebbesen T W 2001 *Phys. Rev. Lett.* **86** 1114
[5] Nezhad M P, Tetz K and Fainman Y 2004 *Opt. Express* **12** 4072
[6] Avrutsky I 2004 *Phys. Rev.* B **70** 155416
[7] Seidel J, Grafstrom S and Eng L 2005 *Phys. Rev. Lett.* **94** 177401
[8] Maier S A 2006 *Opt. Commun.* **258** 259
[9] Ambati M, Nam S H, Ulin-Avila E, Genov D A, Bartal G and Zhang X 2008 *Nano Lett.* **8** 3998
[10] Noginov M A, Zhu G, Mayy M, Ritzo B A, Noginova N and Podolskiy V A 2008 *Phys. Rev. Lett.* **101** 226806
[11] De Leon I and Berini P 2008 *Phys. Rev.* B **78** 161401
[12] Vincenti M A, de Ceglia D, Rondinone V, Ladisa A, D'Orazio A, Bloemer M J and Scalora M 2009 *Phys. Rev.* A **80** 53807
[13] Fang A, Koschny Th, Wegener M and Soukoulis C M 2009 *Phys. Rev.* B **79** 241104
[14] Sivan Y, Xiao S, Chettiar U K, Kildishev A V and Shalaev V M 2009 *Opt. Express* **17** 24060
[15] De Leon I and Berini P 2010 *Nat. Photonics* **4** 382
[16] Bolger P M, Dickson W, Krasavin A V, Liebscher L, Hickey S G, Skryabin D V and Zayats A V 2010 *Opt. Lett.* **35** 1197
[17] Xiao S, Drachev V P, Kildishev A V, Ni X, Chettiar U K, Yuan H-K and Shalaev V M 2010 *Nature* **466** 735
[18] Wuestner S, Pusch A, Tsakmakidis K L, Hamm J M and Hess O 2010 *Phys. Rev. Lett.* **105** 127401
[19] Meinzer N, Ruther M, Linden S, Soukoulis C M, Khitrova G, Hendrickson J, Olitzky J D, Gibbs H M and Wegener M 2010 *Opt. Express* **18** 24140
[20] Tanaka K, Plum E, Ou J Y, Uchino T and Zheludev N I 2010 *Phys. Rev. Lett.* **105** 227403
[21] Stockman M I 2011 *Phys. Rev. Lett.* **106** 156802
[22] Siegman A E 1986 *Lasers* (Mill Valley, CA: University Science Books)
[23] Iizuka K 2002 *Elements of Photonics* vol II (New York: Interscience (Wiley-Interscience))
[24] Shank C V 1975 *Rev. Mod. Phys.* **47** 649
[25] Chang S-H and Taflove A 2004 *Opt. Express* **12** 3827
[26] Bermel P, Lidorikis E, Fink Y and Joannopoulos J D 2006 *Phys. Rev.* B **73** 165125
[27] Bohringer K and Hess O 2008 *Prog. Quantum Electron.* **32** 159
Bohringer K and Hess O 2008 *Prog. Quantum Electron.* **32** 247
[28] Kirby E I, Hamm J M, Pickering T W, Tsakmakidis K L and Hess O 2011 *Phys. Rev.* B **84** 041103
[29] Chua S L, Chong Y D, Stone A D, Soljacic M and Bravo-Abad J 2011 *Opt. Express* **19** 1539
[30] Rodrigo S G, Garcia-Vidal F J and Martin-Moreno L 2008 *Phys. Rev.* B **77** 075401

[31] Porto J A, Garcia-Vidal F J and Pendry J B 1999 *Phys. Rev. Lett.* **83** 2845
[32] Beruete M, Sorolla M, Campillo I, Dolado J S, Martin-Moreno L, Bravo-Abad J and Garcia-Vidal F J 2004 *Opt. Lett.* **29** 2500
[33] Bergman D J and Stockman M I 2003 *Phys. Rev. Lett.* **90** 027402
[34] Zheludev N I, Prosvirnin S L, Papasimakis N and Fedotov V A 2008 *Nat. Photonics* **2** 351
[35] Noginov M A, Zhu G, Belgrave A M, Bakker R, Shalaev V M, Narimanov E E, Stout S, Herz E, Suteewong T and Wiesner U 2009 *Nature* **460** 1110
[36] Oulton R F, Sorger V J, Zentgraf T, Ma R-M, Gladden C, Dai L, Bartal G and Zhang X 2009 *Nature* **461** 629